Applications in Energy and Combustion Science 25 (2026) 100465

Contents lists available at ScienceDirect

Applications in Energy and Combustion Science

journal homepage: www.sciencedirect.com/journal/applications-in-energy-and-combustion-science

Radiative characteristics of premixed ammonia-hydrogen and cracked ammonia swirling flames

Daisuke Sato [a,b,*], Jordan Davies [a], Syed Mashruk [a], Agustin Valera-Medina [a], Ryoichi Kurose [b]

[a] College of Physical Sciences and Engineering, Cardiff University, Wales CF24 3AA, UK
[b] Department of Mechanical Engineering and Science, Kyoto University, Kyoto daigaku-Katsura, Nishikyo-ku, Kyoto 615-8540, Japan

ARTICLE INFO

Keywords:
Zero-carbon
Ammonia
Hydrogen
Cracked ammonia
Turbulent flames
Radiation

ABSTRACT

Renewably produced ammonia does not emit CO_2 with combustion. Therefore, numerous studies have been conducted in recent years to utilise ammonia as a carbon free fuel. However, there is limited previous knowledge regarding the radiation characteristics of ammonia blend combustion. In this study, radiation characteristics are investigated for 15 kW premixed swirling flames of NH_3/H_2 (70/30) and 20% cracked NH_3, which have been frequent targets of recent research, with equivalence ratios varying from $0.6 \leq \Phi \leq 1.4$. Specifically, water radiation (wavelength 2.7 μm), which is the main radiation source, is measured using an infrared spectrometer. Additionally, radiation emission and absorption in the combustor are evaluated theoretically using H_2O exhaust gas concentrations and temperature measurement data. The results suggest that radiation changes due to equivalence ratio variations are gradual on the rich side, showing different trends compared to the lean side. Furthermore, radiation attenuation in the combustor become active around $\Phi = 0.9$. This suggests that when considering radiation in ammonia blend combustion, not only the blend composition but also equivalence ratio conditions must be carefully considered. In addition, radiative heat fluxes were analysed for three blends (NH_3/H_2, pure NH_3, and cracked NH_3) at $\Phi = 1.0$, suggesting no significant differences in radiative heat flux among these blends. These research findings provide valuable insights for future combustor designs using ammonia blend fuels.

1. Introduction

Because of its high energy density and ease of transportation and handling, ammonia is gaining attention as a sustainable energy carrier [1]. Furthermore, because ammonia is carbon-free and does not emit CO_2 when burned, research on using ammonia as a carbon-free fuel has been actively explored in recent years [2,3]. However, ammonia combustion has challenges, such as NOx emissions and low reactivity [4]. Therefore, an NH_3/H_2 blend containing highly reactive hydrogen has been devised. Additionally, $NH_3/H_2/N_2$ blend, produced by thermal decomposition of part of the ammonia using waste heat from the combustor, has been proposed as an industrially preferable option to avoid using hydrogen which has high purification costs [5–7]. There has been a lot of research published on the combustion characteristics of these blend fuels, such as NOx emissions [8,9].

However, there is limited knowledge on the radiative characteristics of NH_3/H_2 and cracked NH_3 blend combustion. Clarifying the radiative characteristics would be extremely beneficial as they are crucial factors in designing industrial furnaces for material heating and gas turbine combustors for liner cooling [10]. The study by Murai et al. [11,12] is one of the experimental investigations into the radiative characteristics of ammonia combustion. Their research measured the total radiative heat flux and infrared spectrum for non-premixed combustion in a 10 kW test furnace. The results demonstrated that ammonia combustion exhibited approximately 22 % lower radiative heat flux compared to methane combustion, while oxygen-enriched ammonia combustion (30 vol.% oxygen) exhibited higher radiative heat flux than methane combustion. Furthermore, it was revealed that 95 % of the total radiative heat originated from furnace walls, indicating that radiation from the furnace walls is more significant than direct flame radiation in industrial furnace heating. Zheng et al. [13] investigated the impact of ammonia addition on the flame emissivity of hydrocarbon fuels (CH_4, C_2H_4) in jet flames using a radiometer. Their findings confirmed a decrease in emissivity with increasing ammonia blending ratio. By normalising the measured results with the emissivity of pure hydrocarbon flames, they elucidated the influence of ammonia addition and proposed a model

* Corresponding author at: College of Physical Sciences and Engineering, Cardiff University, Wales CF24 3AA, UK.
E-mail address: satod@cardiff.ac.uk (D. Sato).

https://doi.org/10.1016/j.jaecs.2026.100465
Received 27 September 2025; Received in revised form 17 January 2026; Accepted 20 January 2026
Available online 21 January 2026

describing its impact on emissivity using the Reynolds number. Fang et al. [14] examined the variations in flame emissivity, shape factor, and radiative heat flux at different flow rates of ammonia and methane or propane. Their results indicated a decrease in flame emissivity, shape factor, and radiative heat flux with increasing ammonia blending ratio. Based on these findings, they developed a predictive correlation for thermal radiation as a function of flame height and width. These investigations provided valuable insights into the radiative characteristics of pure ammonia or ammonia/hydrocarbon blended fuels. However, the radiative characteristics of NH_3/H_2 or cracked NH_3 flames remain experimentally unexplored.

Furthermore, several previous studies using numerical analysis have reported that radiation not only heats materials but also affects reactions in ammonia flames. Nakamura et al. [15] computationally demonstrated that flame temperature variations due to radiative heat loss in laminar premixed pure ammonia flames affected laminar burning velocity and emissions like NO and unburned ammonia. Fang et al. [16] investigated counterflow premixed ammonia-air flame extinction in high-pressure systems up to 5 atm using numerical simulations and partially validated their findings with experiments. Their results elucidated the impact of radiative heat loss on flame extinction, particularly under lean conditions. Zheng et al., [17] through computational analysis, showed that radiation reabsorption in laminar NH_3/H_2 flames influenced H, OH, and NH_2 radical concentrations, consequently impacting laminar burning velocity. Furthermore, they revealed that the influence mechanism changed around an equivalence ratio of 1.25. Another study by Zheng et al. [18] computationally demonstrated that increasing hydrogen content in laminar NH_3/H_2 flames reduced the impact of radiation reabsorption on laminar burning velocity and NO emissions. De Gioegi et al. [19] evaluated the influence of radiation models on performance predictions for a micro combustor for micro thermophotovoltaic (MTPV) applications. Comparing a multispecies Planck-mean approximation radiation model (PMAC), a narrowband model for water vapor, and a scenario excluding radiation effects, they showed that radiation variations due to changes in equivalence ratio and hydrogen concentration affected the calculated results of flame length and laminar flame speed.

As demonstrated above, while thermal radiation was known to influence ammonia blend flame characteristics, directly experimental investigations into the radiative characteristics of ammonia blend flames across various equivalence ratios were lacking. The accumulation of fundamental data in this study is of paramount importance from both practical and numerical analysis perspectives. In the absence of the experimental evidence presented in this study, numerical simulations of ammonia blend combustion risk overlooking radiative effects. Such an oversight could lead to significant inaccuracies in the prediction of flame speeds and NOx formation. Furthermore, without quantitative experimental benchmarks, combustor designers would be forced to rely on inappropriate hydrocarbon-based empirical correlations, potentially resulting in suboptimal thermal management and compromised system efficiency in future ammonia combustors. Industrially, it contributes to the optimisation of heating efficiency in industrial furnaces and the refinement of thermal load predictions in gas turbine combustors, serving as critical design guidelines for retrofitting existing facilities for ammonia blended fuel. Meanwhile, from an academic and analytical standpoint, it functions as a validation database for radiation models in CFD simulations. In particular, accurately characterising water-vapor-dominated radiative properties improves the prediction accuracy of NOx formation and extinction limits, which are affected by radiative heat loss. This is expected to enhance the reliability of computational design for high-efficiency combustion systems.

This study represents a logical progression from the authors' preceding work. A prior investigation into the complex radiative environment of coke oven gas-ammonia ($COG//NH_3$) flames [20] demonstrated that although H_2O is the principal radiating species, fluctuations in radiation resulting from changes in the fuel mixture are predominantly governed by CO_2 concentration. Considering this finding, the present study was designed to elucidate the fundamental radiative physics of H_2O generated in ammonia-blend flames. By utilizing the same validated experimental platform while shifting to carbon-free fuels (NH_3/H_2 and cracked NH3), this methodology facilitates a focused investigation into the radiative dynamics of H_2O, specifically the phenomena of emission and attenuation.

Therefore, this study investigated the radiative characteristics of NH_3/H_2 and cracked NH_3 premixed swirling flames, commonly used in recent ammonia blend combustion research, under varying equivalence ratios. Specifically, the water radiation, the primary source of radiation in these blended fuel flames, was measured using an infrared spectrometer. Furthermore, theoretical analysis utilising the measured H_2O exhaust gas concentration and temperature data was conducted to evaluate radiation emission and reabsorption. Additionally, using the theoretical analysis method whose reliability was confirmed in the above investigation, further combustion experiments were conducted at Φ=1.0 for CH_4 and pure NH_3, in addition to NH_3/H_2 and cracked NH_3. The changes in radiative characteristics due to variations in these blends were also evaluated.

2. Experimental setup and methodology

2.1. Tangential swirl burner

The experiments were conducted using a tangential swirl combustor (Sg = 1.45 with long nozzle) under atmospheric conditions (1.1 bar and 288 K), as shown in Fig. 1. Detailed specifications and dimensions of the burner geometry, including the swirler design, and the flame geometry have been described in the previous work [21]. Fuel and air were injected into the premixing chamber and passed through a radial tangential swirler to form a swirl flame. To enable spectroscopic measurements of the flame, a cylindrical GE214 quartz tube (d = 156 mm, h = 300 mm) was used to confine the swirl flame. This quartz tube had sufficiently high transmittance of over 90 % in the infrared wavelength range (2.5–3.0 μm) measured in this study. The ammonia fraction in the NH_3/H_2 blend was set to 0.7. For the cracked ammonia blend ($NH_3/H_2/N_2$), a 20 % cracked blend (0.667/0.25/0.083) was adopted. This blend was selected to have a similar ammonia fraction to NH_3/H_2 for comparison purposes. Bronkhorst mass flow controllers were used to control the gas flow rates of ammonia, hydrogen, nitrogen, and air (accuracy better than ±0.5 % within 15–95 % of the full scale). Experiments were conducted across an equivalence ratio range of $0.6 \leq \Phi \leq 1.4$ while maintaining 15 kW for all blends by varying the volumetric flow rates of fuel and air. The Reynolds numbers of the bulk flow in the quartz tube ranged from 640 to 1270 under the experimental conditions. Given that these values are within the laminar regime (Re < 2300), the flow in the post-flame zone was assumed to be fully developed laminar flow for the purpose of heat transfer correction. The uncertainty in the equivalence ratio was estimated based on the accuracy of the mass flow controllers (±0.5 %). Using the root sum of squares (RSS) propagation method, the combined uncertainty for the equivalence ratio is calculated to be approximately ±0.7 %.

2.2. Measurements methods

2.2.1. Temperature measurements

The exhaust gas temperature at a point 50 mm upstream from the exit in the quartz tube was measured using an R-type sheathed thermocouple. Additionally, the outer wall temperature of the quartz tube at the same height was measured using a K-type sheathed thermocouple. The measurement data was recorded at 1 Hz after confirming that the temperature had stabilized under each condition, and 60 s of data was averaged. Since the exhaust gas temperature was high, the energy loss due to radiation from the thermocouple to the surroundings could not be ignored. Therefore, the numerical heat transfer correction method

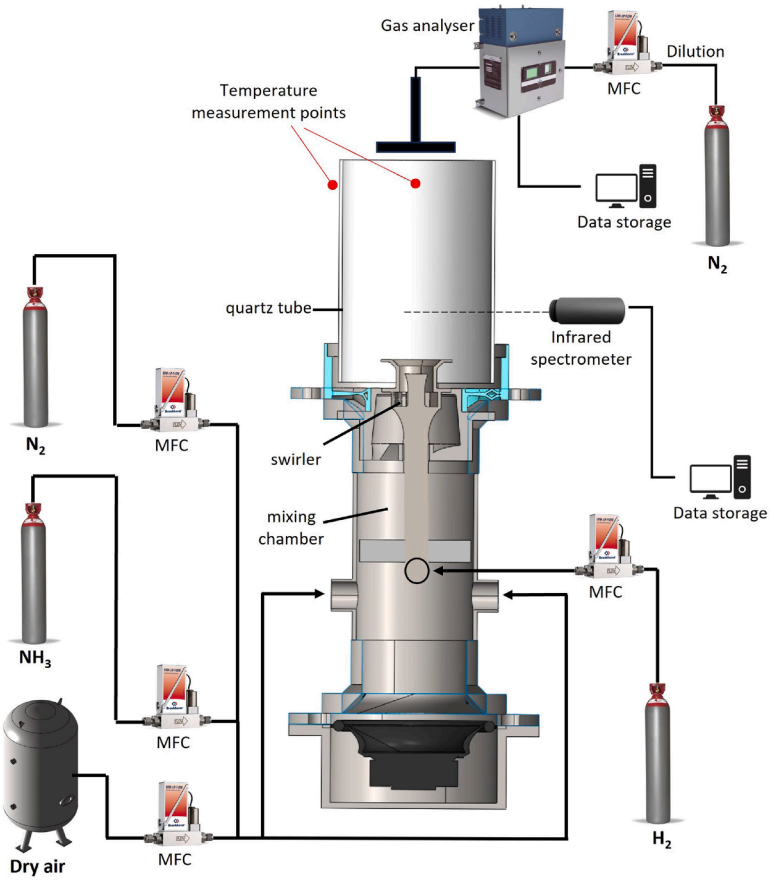

Fig. 1. Schematic of experimental system.

(HTM) used by Cafiero et al. [22] was applied to the exhaust gas temperature to correct for radiation. The convective heat transfer coefficient used in this correction was calculated using the empirical correlation proposed by Kramers [23], which is a function of Reynolds (*Re*) and Prandtl (Pr) numbers. Although the intrinsic accuracy of the thermocouple is high (±1.5 K), the radiation correction introduces additional uncertainty dependent on the estimated heat transfer coefficient. Assuming a conservative uncertainty of 20 % for heat transfer coefficient, the combined uncertainty for the corrected gas temperature is estimated to be approximately ±30 K (about ±2.5 %). Consequently, temperature values reported in this study are rounded to the nearest 10 K to reflect this precision.

2.2.2. Exhaust gas emission analysis

The exhaust gases (H_2O and NH_3) were measured using an Emerson CT5100 Quantum Cascade Laser analyser capable of measuring at 1 Hz (with ±1 % reproducibility and 0.999 linearity). A cross-shaped probe with equally spaced holes was placed at the outlet of the quartz tube to collect sample gas for analysis, ensuring uniform sampling. The sample line was heated to 463 K to prevent condensation and minimise sampling losses. N_2 dilution with ±10 % reproducibility was used for points exceeding the analyser's detection limits. Regarding the measurement uncertainty, the manufacturer's nominal error (±1 %) represents only the instrumental precision. A more comprehensive assessment was conducted using the RSS method, accounting for the calibration gas uncertainty (±0.5 %) and potential sampling system biases. Based on this, the combined uncertainty for direct measurements is conservatively estimated to be within ±2.0 %. However, for the data points requiring N2 dilution, the overall uncertainty is dominated by the dilution process, estimated at approximately ±10 %. 120 points were acquired for each test condition and time averaged. Since the radiative characteristics of each gas component were based on concentration, the obtained results were used for radiation evaluation.

NOx component analysis was also conducted simultaneously using the gas analyser. NO, which accounted for the majority of the NOx, peaked at $\Phi = 0.9$ for both NH_3/H_2 and cracked NH_3 blends, with concentrations decreasing under leaner or richer conditions. However, even at this maximum NO concentration (NH_3/H_2 flame at $\Phi = 0.9$), the value was 3714 ppm (wet), which was extremely low compared to the H_2O concentration exceeding 20vol %. Consequently, the contribution of NOx to the radiative characteristics of the combustor was considered sufficiently low under the experimental conditions, and thus these results were omitted from this paper.

2.2.3. Infrared spectrometry measurements

The radiation from the flame was measured using an infrared spectrometer (NLIR S2050–400). Although this spectrometer could measure in the wavelength range of 2.0–5.0 μm with a resolution of 6 cm^{-1}, this study focused on the 2.5–3.0 μm range, which includes the water radiation wavelength of 2.7 μm [24]. The spectrometer was positioned 0.35 m away from the outer wall of the quartz tube, at heights of 40 mm, 80 mm, and 180 mm from the burner exit for each experimental condition. A reflective collimator (THORLABS RC12SMA-P01) was attached to the sensor's tip to limit the field of view. Parallel radiation was collected at each height within a maximum beam diameter of $\phi = 22$ mm. The exposure time was set to 570 ms, and 20 scans were averaged. Fig. 2 shows an example of spectrometry measurements in the 2.5–3.0 μm range, obtained using an infrared spectrometer at various heights (NH_3/H_2, $\Phi = 1.0$). Measurements at heights of 40 mm and 80 mm captured radiation from the flame zone (FZ), while measurements at 180 mm captured radiation from the post flame zone (PFZ). The dashed line represented background radiation from the heated quartz tube and

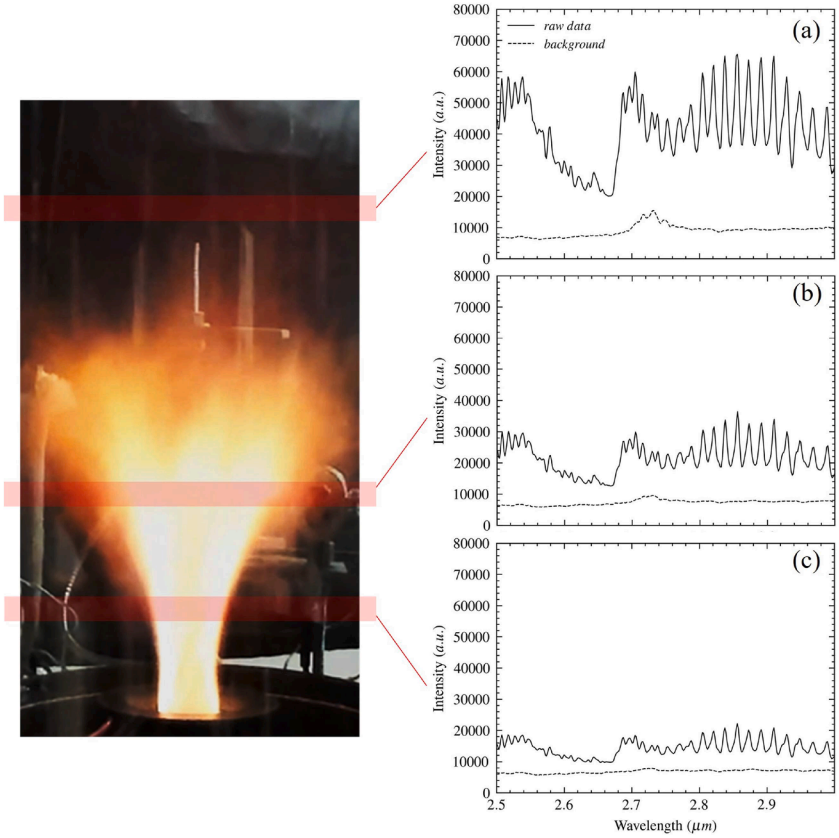

Fig. 2. Example of infrared spectrometry data (Φ = 1.0 and NH_3/H_2 (70/30) condition) at (a) 180 mm, (b) 80 mm and (c) 40 mm height from burner nozzle.

ambient air, obtained by extinguishing the flame while the quartz tube was hot and quickly purging the tube with air. In this study, the intensity at 2.7 μm, the emission wavelength of water, was extracted for each experimental condition after subtracting the background, and radiative characteristics were evaluated.

2.3. Internal radiation theoretical analysis methods

In addition to the evaluation using infrared spectrometry data, internal radiation theoretical analysis was conducted using temperature and exhaust gas emission measurement data. Fig. 3 schematically shows the heat transfer around PFZ in this study. The inner wall of the quartz tube was heated by the radiative heat flux (Q_r) and the convective heat flux (Q_h) from the combustion gas, which raised the temperature of the quartz tube inner wall.

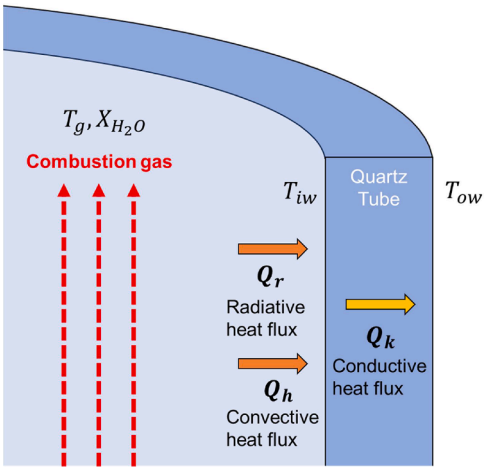

Fig. 3. Schematic diagram of heat flux in quartz tube.

Q_r could be approximated by a method developed by Hottel and Egbert [25,26] as follows:

$$Q_r = 0.5(1+\varepsilon_w)\sigma\left(\varepsilon_g {T_g}^4 - \alpha_g {T_{iw}}^4\right)A_{iw} \quad (1)$$

where ε_w was the emissivity of the quartz tube, σ was the Stefan-Boltzmann constant, T_g was the exhaust gas temperature, T_{iw} was the quartz tube inner wall temperature, and A_{iw} was the area of the quartz tube inner wall. ε_g and α_g represented the emissivity and absorptivity of the combustion gas, respectively. This method was originally developed for hydrocarbon combustion. However, since the ammonia blended combustion targeted in this study did not produce CO_2, the emissivity and absorptivity could be obtained as follows:

$$\varepsilon_g = C_{H2O}\varepsilon_{H2O} \quad (2)$$

$$\alpha_g = \alpha_{H2O} = C_{H2O}\varepsilon'_{H2O}\left(\frac{T_{iw}}{T_g}\right)^{0.45} \quad (3)$$

The emissivity of H_2O (ε_{H2O}) could be obtained from Hottel's charts [25,26] based on temperature and beam length. C_{H2O} was correction factors that considered the partial pressures of H_2O. This value could be obtained from Hottel's charts based on temperature and partial pressure data.

Q_h could be expressed by the following equation:

$$Q_h = h\left(T_g - T_{iw}\right)A_{iw} \quad (4)$$

where h was the heat transfer coefficient, and its value could be approximately determined as Nu = 4.36 under the assumption of a circular pipe with constant wall heat flux [27].

Furthermore, a temperature difference occurred between the inner

and outer walls of the quartz tube due to heat conduction from the inner wall to the outer wall. In this case, the conductive heat flux (Q_k) passing through the quartz tube could be described as follows:

$$Q_k = \frac{2\pi Lk}{\ln\frac{r_2}{r_1}}(T_{iw} - T_{ow}) \tag{5}$$

where L was the height of the quartz tube, k was the thermal conductivity of the quartz tube, r_1 and r_2 were the inner and outer diameters of the quartz tube, and T_{ow} was the outer wall temperature of the quartz tube.

At this situation, the following relationship holds from the heat flux balance:

$$Q_k = Q_r + Q_h \tag{6}$$

In the experimental measurements of this study, the exhaust gas temperature, emissions in the exhaust gas, and the outer wall temperature of the quartz tube were measured, so only the inner wall temperature of the quartz tube was unknown. This inner wall temperature could be determined by substituting Eqs. (1), (4), and (5) into Eq. (6) and performing a loop calculation, and each heat flux could also be obtained. Using this method, Q_r under each experimental condition was obtained and the radiative characteristics were evaluated.

To supplement the validity of the Hottel model adopted in this study, the author's previous research [20] confirmed its effectiveness for evaluating the radiation characteristics of COG/NH_3 blended fuels through a comparison with Line-by-Line (LBL) calculations. However, the same study also revealed a slight tendency to overestimate the radiative heat flux under conditions with a high hydrocarbon content (the source of CO_2) and a low ammonia fraction. Conversely, the model was confirmed to have high accuracy under conditions with a high ammonia fraction. Because the fuel blends targeted in the present study are hydrocarbon-free and do not produce CO_2 in the exhaust gas, the source of uncertainty identified in the prior work is eliminated, allowing the Hottel model to be applied with higher reliability. Accordingly, the theoretical analysis in this study is based on the Hottel model, and its evaluation is conducted through comparison and verification with the experimental spectroscopic measurements.

2.4. Comparative evaluation of CH_4 and NH_3 radiative heat flux using emissions measurements and theoretical analysis

Additional experiments were conducted to compare the radiative heat flux of the NH_3/H_2 and cracked NH_3 blends, which were the main targets of this study, with conventional CH_4 and pure NH_3 ($\Phi = 0.9$, 15 kW). Regarding the CH_4 measurements, infrared spectrometry analysis was unfortunately not performed because the quartz tube used in the experiments exhibited a sharp decrease in transmittance at wavelengths above 3.5 μm, making it impossible to evaluate CO_2 radiation. While spectrometry measurements for pure NH_3 were feasible, they were not conducted in this study as reliable data already exists in the literature [11,12], and the primary focus of this work is on ammonia blends. Therefore, a comparative evaluation of the radiative heat flux for the four types of fuels was conducted by additionally measuring the exhaust H_2O concentrations and temperatures of the CH_4 and pure NH_3 flames, and applying the internal radiation theoretical analysis validated with NH_3/H_2 and cracked NH_3.

3. Results and discussion

3.1. Exhaust gas temperature

The radiation corrected exhaust gas temperatures and quartz tube wall temperatures were shown in Figs. 4 and 5, respectively. The exhaust gas temperature peaked at $\Phi = 0.9$ for both blends, with NH_3/H_2 reaching a maximum of 1310 K and cracked NH_3 reaching a maximum of 1270 K. NH_3/H_2 showed higher exhaust gas temperatures than cracked NH_3 throughout the entire range, not just at $\Phi = 0.9$. This difference was particularly pronounced under lean conditions, likely due to the dilution effect of nitrogen present in the cracked NH_3 blend. Furthermore, both blends exhibited that the change in exhaust gas temperature was more gradual on the rich side compared to the lean side. This indicated that the temperature decreased due to the increasing fraction of air on the lean side was more rapid than the temperature drop caused by insufficient air for combustion on the rich side. Regarding the inner and outer wall temperature, the inner wall temperature was higher than the outer wall temperature as expected. No significant temperature change due to the change in equivalence ratio was confirmed.

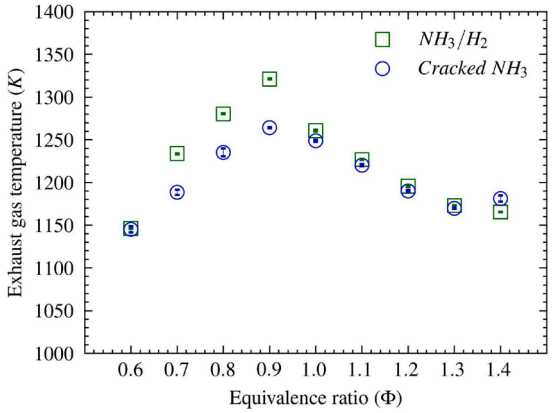

Fig. 4. Exhaust gas temperature results.

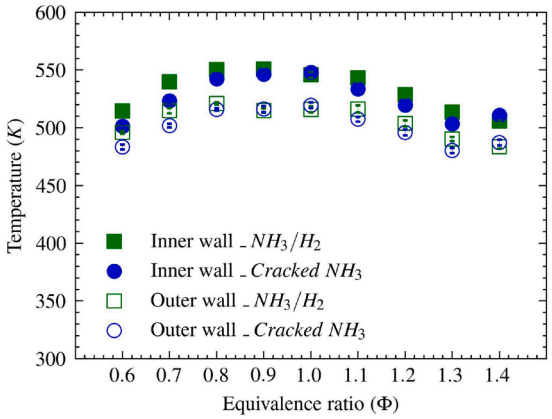

Fig. 5. Quartz tube wall temperature results.

3.2. Emissions analysis of H_2O and NH_3

The exhaust gas analysis results of H_2O and NH_3 emissions were shown in Figs. 6 and 7. H_2O emission was found to peak at Φ=0.9 for both blends. NH_3/H_2 showed higher H_2O emissions than cracked NH_3 across all equivalence ratios. Additionally, both blends exhibited a more gradual change in H_2O emission on the rich side compared to the lean side. This indicated that the decrease in H_2O concentration due to increasing air fraction in the exhaust gas on the lean side was more rapid than the decrease in H_2O emission caused by insufficient air for combustion on the rich side. As mentioned above, the H_2O emission trend was shown to be similar to the exhaust gas temperature trend.

Furthermore, unburned NH_3 emission increased sharply under fuel-rich conditions above Φ = 0.9–1.0. However, under conditions that could be analysed with the analyser, the maximum emission was around 1500 ppm at $\Phi = 1.1$. In previous literature [28], simulations for pure

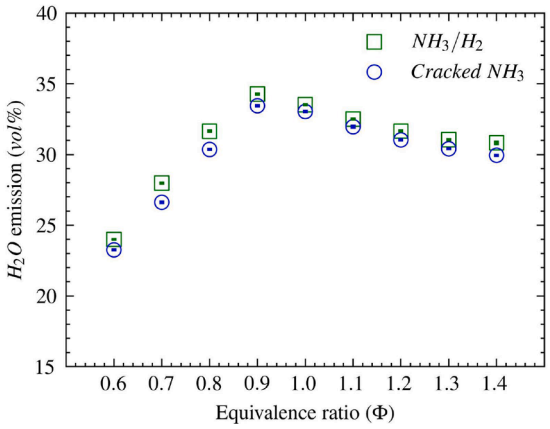

Fig. 6. H_2O emission analysis results.

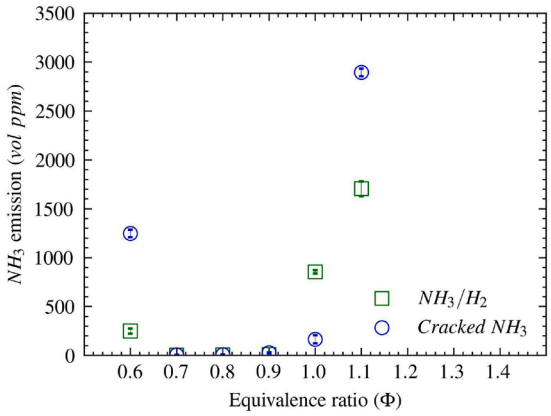

Fig. 7. NH_3 emission analysis results.

NH_3 combustion at Φ=1.4, which was expected to have higher NH_3 slip, showed unburned NH_3 emissions of around 10,500 ppm. This indicated that unburned NH_3 emissions accounted for less than 3.4 % of the H_2O emissions obtained in this experiment. Since NH_3/H_2 and cracked NH_3 combustion did not produce CO_2, the main radiation sources were considered to be H_2O and NH_3. However, the fraction of NH_3 in the exhaust gas was very small compared to H_2O, and a previous study [20] reported that the radiative contribution of NH_3 was 3 % or less of that of H_2O. Therefore, the effect of ammonia on radiation was assumed to be negligible in this study.

3.3. Infrared spectrometry analysis

The count intensity at 2.7 μm, after background correction, for each condition of NH_3/H_2 and cracked NH_3 blends are shown in Fig. 8. Overall, water radiation increased with distance from the burner exit, reaching its maximum at a height of 180 mm in the PFZ. The intensity at the PFZ (180 mm point) was approximately 5 times higher than that at the 40 mm point, and about 2.5 times higher than at the 80 mm point in the FZ. This indicated that radiation from the PFZ was dominant within the combustor. This was presumed to be due to the high presence of H_2O, which was the main radiation source produced by the completion of combustion reactions, in the PFZ downstream of the FZ.

Furthermore, it was found that water radiation peaked around Φ = 0.9–1.0, similar to the temperature measurements and H_2O emissions. Overall, it was confirmed that the radiation from cracked NH_3 tended to be slightly weaker compared to the NH_3/H_2 blend. This was thought to be due to the dilution effect of N_2 present in the fuel blend.

Moreover, the measurement results also confirmed that the variation in radiation due to changes in the equivalence ratio was more gradual on the rich side compared to the lean side. This correlated well with the measurement results for exhaust gas temperature and H_2O emissions.

These results suggested that careful consideration should be given not only to the blend composition but also to the equivalence ratio conditions when considering radiation in the design of burners utilizing ammonia blended fuels.

As stated in Section 2.3, the radiation intensity is primarily dependent on the H_2O concentration and the fourth power of the combustion gas temperature. Therefore, to decouple these dominant thermal and concentration effects and evaluate the intrinsic radiative properties (i.e., effective emissivity and absorption capabilities) of the flame gas, the infrared spectrometry measurement results were normalised using the H_2O emission and the fourth power of the gas temperature, as shown in Eq. (7):

$$\textit{Per unit } H_2O \textit{ radiation} = \frac{I_{H2O}}{X_{H2O} \cdot T_g^{\,4}} \tag{7}$$

where I_{H2O} represented the infrared spectrometry measurement data shown in Fig. 8, and X_{H2O} represented the measured H_2O emission shown in Fig. 6. Since H_2O emission sampled from the exhaust gas at the

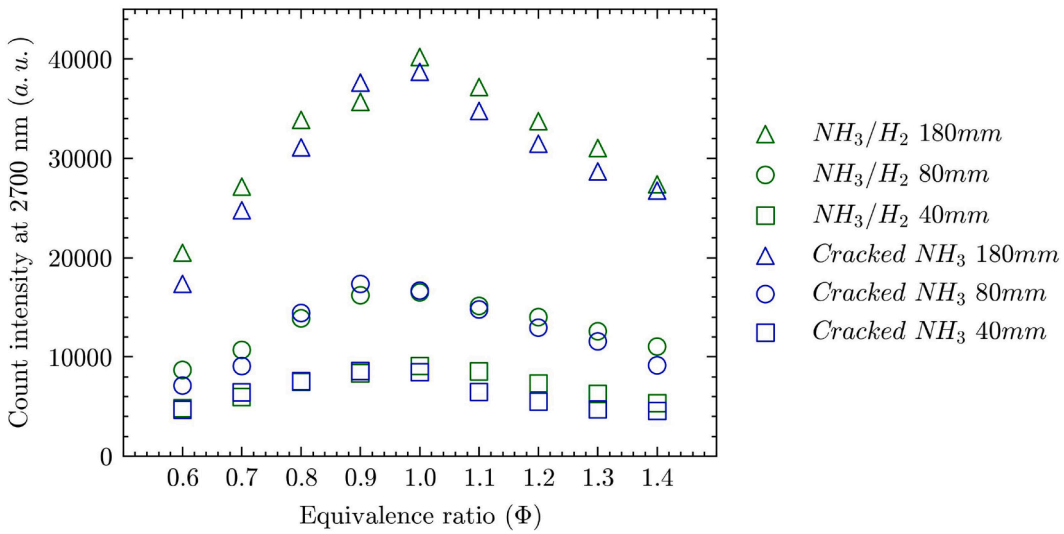

Fig. 8. Raw count intensity at 2.7 μm measured by infrared spectrometer.

quartz tube exit was used for this normalisation, the per-unit H_2O radiation evaluation was conducted only for infrared spectrometry measurements in the PFZ (height 180 mm). The values presented in Fig. 9 are dimensionless ratios normalised by the global maximum value in the dataset. This normalisation highlights the relative variation in radiative attenuation independent of absolute intensity scales. The results indicated that the per-unit H_2O radiation reached its minimum around Φ=0.9. Conversely, as the equivalence ratio shifted towards the lean or rich side, the per-unit H_2O radiation increased. This suggested that some form of radiative attenuation, including the reabsorption of H_2O radiation, may be intensifying around $\Phi = 0.9$. In contrast, when the equivalence ratio shifted to the lean or rich side, the emission of H_2O radiation became more significant.

3.4. Internal radiation theoretical analysis

The radiative heat flux to inner wall calculated by internal radiation theoretical analysis for each condition of NH_3/H_2 and cracked NH_3 blends are shown in Fig. 10. The radiative heat flux to the inner wall was found to peak at $\Phi = 0.9$, similar to the temperature, H_2O emission, and infrared spectrometry measurement results. Overall, the radiation from the cracked NH_3 tended to be slightly weaker compared to the NH_3/H_2 blend. Furthermore, the difference in radiative heat flux between the NH_3/H_2 blend and the cracked NH_3 was larger on the leaner side than at $\Phi = 0.9$. This was thought to be due to the dilution effect of N_2 contained in the fuel blend, and in particular, the dilution effect of gas temperature was considered to have a large influence from the results of Fig. 4. The measurement results also confirmed that the change in radiative heat flux due to the change in equivalence ratio was more gradual on the rich side than on the lean side. This showed a good correlation with the infrared spectrometry measurement results, demonstrating the reliability of both results obtained by different methods.

As stated in Section 2.3, this internal radiation theoretical analysis used Eq. (1), which consisted of radiation emission and absorption terms. Therefore, by calculating only the radiation absorption term as shown in Eq. (8), it was possible to approximate the radiation absorbed.

$$Q_{r\_absorb} = 0.5(1+\varepsilon_w)\sigma\alpha_g T_{iw}{}^4 A_{iw} \quad (8)$$

The calculated absorbed radiative heat flux is shown in Fig. 11. The results showed that the absorbed radiative heat flux peaked at Φ=0.9 for both blends. In addition, the absorbed radiative heat flux of the NH_3/H_2 blend was greater than that of cracked NH_3 at leaner conditions than $\Phi = 0.9$. This showed the same trend as the per-unit H_2O radiation obtained using infrared spectrometry measurements, demonstrating the reliability of both results, obtained by different methods, for the evaluation of absorbed radiation.

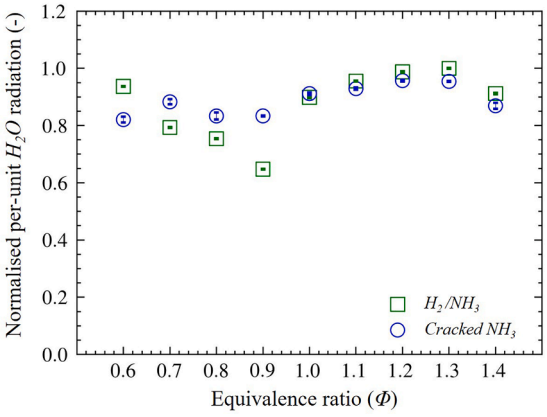

Fig. 9. Normalised per-unit H_2O radiation (Spectral intensity at 2.7 μm normalised by the fourth power of exhaust gas temperature and H_2O concentration).

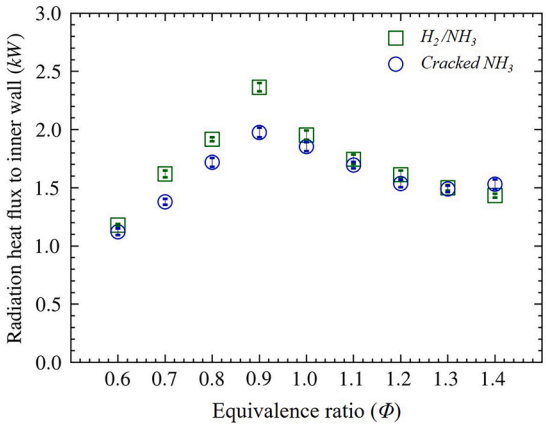

Fig. 10. Radiative heat flux to inner wall calculated by theoretical analysis method.

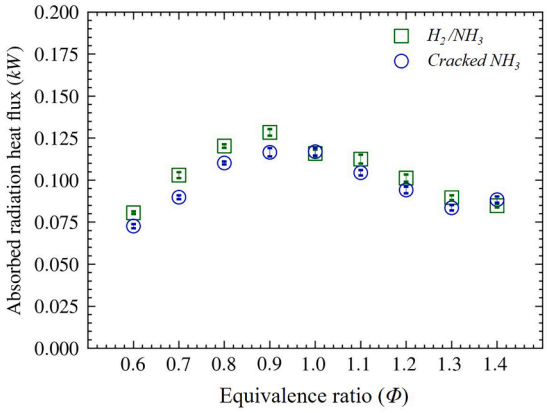

Fig. 11. Absorbed radiative heat flux in the combustor calculated by theoretical analysis method.

The radiation absorption trend with a peak at $\Phi = 0.9$, confirmed by both infrared spectrometry and theoretical analysis, provides the first experimental evidence in turbulent swirling flames that supports the numerical predictions by Zheng et al. [17,18]. Their computational work on laminar flames proposed that radiation reabsorption-induced chemical effects become dominant in NH_3/H_2 flames. Our findings suggest that this phenomenon is not limited to laminar flames but is also a critical factor in more practical turbulent combustion regimes. Therefore, our experimental results strongly support the possibility that key radicals such as H, OH, and NH_2 are significantly affected by radiation within this active absorption region, providing a crucial validation target for future high-fidelity combustion models.

3.5. Comparison of radiative heat fluxes using four different blends

The radiative heat flux to the inner wall for the four blends at $\Phi = 1.0$ and 15 kW, as calculated from the additional experimental results using internal radiation theoretical analysis are shown in Fig. 12. In addition, a zero-dimensional equilibrium calculation using Okafor et al.'s mechanism [29] was performed to discuss the radiation differences between fuels, and these results are also shown in Fig. 12. CH_4 exhibited a heat flux approximately 25 % greater than the ammonia blend fuels. This result was consistent with previous studies [11,12] using radiometer measurements. Furthermore, the radiative heat flux among the three ammonia blended fuels was shown to slightly decrease in the order of NH_3/H_2 > NH_3 > 20 % cracked NH_3. This appears to contradict the trend of equilibrium flame temperature, which shows that cracked NH_3

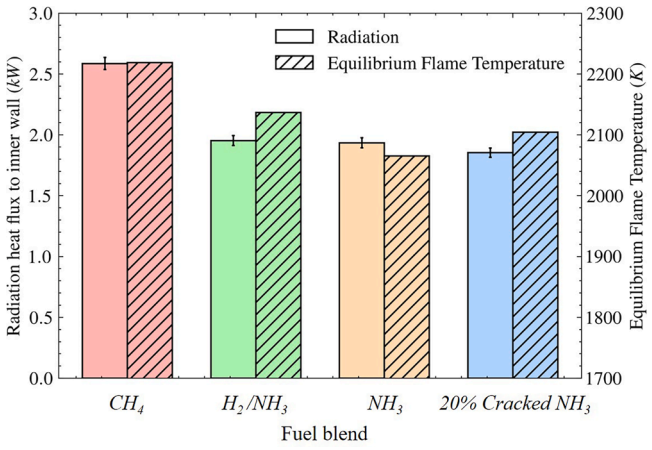

Fig. 12. Radiation heat flux to the inner wall obtained by internal radiation theoretical analysis and calculated equilibrium flame temperature of the four blends at $\Phi = 1.0$.

flames have higher values than NH_3 flames. However, this is within the uncertainty range (2.0 %) of the methodology, indicating that the radiative heat fluxes for different ammonia blends are very close. Thus, it was quantitatively demonstrated that not only pure NH_3, which has been experimentally investigated in the past [11,12], but also ammonia blended fuels such as NH_3/H_2 and cracked NH_3 produce lower radiative heat fluxes than methane. This is a crucial point for using these mixtures via the retrofitting of methane systems, suggesting that more fuel or higher efficiency might be needed to address the reduction in radiative heat flux.

4. Conclusions

In this study, the radiative characteristics of NH_3/H_2 and cracked NH_3 premixed swirling flames were experimentally investigated using infrared spectrometry and internal radiation theoretical analysis under various equivalence ratios.

- The exhaust gas temperature and H_2O concentration, which have a significant impact on radiation, are found to be generally higher in NH_3/H_2 flames compared to cracked NH_3 flames, peaking around $\Phi = 0.9$. For both blends, temperature and H_2O emission changes are more gradual on the rich side compared to the lean side.
- Infrared spectrometry results reveal that radiation from water vapor generally increases with distance from the burner exit, indicating that radiation from the PFZ is dominant within the combustor.
- Both infrared spectrometry and internal radiation theoretical analysis reveal that radiation peaks around $\Phi = 0.9$–1.0, with more gradual changes on the rich side compared to the lean side.
- Per-unit H_2O radiation analysis based on infrared spectrometry results and internal radiation theoretical analysis suggest that H_2O radiation attenuation is active around $\Phi = 0.9$. As the equivalence ratio shifts to the lean or rich side, the emission of H_2O radiation outside the flame becomes dominant.
- The good agreement between the results obtained from both infrared spectrometry and internal radiation theoretical analysis are confirmed.
- Additional internal radiation theoretical analysis confirmed that the radiative heat flux to the inner wall for various ammonia blends (NH_3/H_2, pure NH_3, and cracked NH_3) is lower than that of CH_4, while suggesting for the first time that there is no significant difference among these ammonia blends.

This study was the first to experimentally investigate the radiative characteristics of various ammonia blended fuels. The findings suggested that when considering radiation in ammonia blend combustion, not only the blend composition but also the equivalence ratio conditions need to be carefully considered. These results provided valuable insights for the future design of combustors utilizing ammonia blended fuels.

CRediT authorship contribution statement

Daisuke Sato: Writing – original draft, Visualization, Project administration, Methodology, Investigation, Data curation. **Jordan Davies:** Writing – review & editing, Investigation, Data curation. **Syed Mashruk:** Writing – review & editing, Supervision. **Agustin Valera-Medina:** Writing – review & editing, Supervision. **Ryoichi Kurose:** Writing – review & editing, Supervision.

Declaration of competing interest

The authors declare that they have no known competing financial interests or personal relationships that could have appeared to influence the work reported in this paper.

Acknowledgements

The work was supported by Project AMBURN with funding from the Department for Energy Security & Net Zero (DESNZ) under award no. IFS2-06-FLO and Nippon Steel Corporation. The experimental work was undertaken at Cardiff University's Thermofluids lab (W/0.17) with invaluable technical support from Mr. Jonathan Martin. For the purpose of open access, the author has applied a CC BY public copyright licence to any Author Accepted Manuscript version arising.

Data availability

Data will be made available on request.

References

[1] Kobayashi H, Hayakawa A, Somarathne K, Okafor EC. Science and technology of ammonia combustion. Proc Combust Inst 2019;37:109–33.
[2] Valera-Medina A, Amer-Hatem F, Azad AK. Review on ammonia as a potential fuel: from synthesis to economics. Energy Fuel 2021;35:6964–7029.
[3] Valera-Medina A, Xiao H, Owen-Jones M, David WIF, Bowen PJ. Ammonia for power. Prog Energy Combust Sci 2018;69:63–102.
[4] Li J, Huang H, Kobayashi N, He Z, Nagai Y. Study on using hydrogen and ammonia as fuels: Combustion characteristics and NOx formation. Int J Energy Res 2014;38:1214–23.
[5] Asif M, Sidra Bibi S, Ahmed S, Irshad M, Shakir Hussain M, Zeb H, et al. Recent advances in green hydrogen production, storage and commercial-scale use via catalytic ammonia cracking. Chem Eng J 2023;473:145381.
[6] Davies J, Mashruk S, Sato D, Mazzotta L, Pugh D, Valera-Medina A. Emissions analyses of humidified cracked ammonia swirling flames. Combust Flame 2025;274:113984.
[7] An Z, Zhang W, Zhang M, Xing J, Kai R, Lin W, et al. Experimental and numerical investigation on combustion characteristics of cracked ammonia flames. Energy Fuels 2024;38:7412–30.
[8] Khateeb AA, Guiberti TF, Wang G, Boyette WR, Younes M, Jamal A, et al. Stability limits and NO emissions of premixed swirl ammonia-air flames enriched with hydrogen or methane at elevated pressures. Int J Hydrog Energy 2021;46:11969–81.
[9] Mashruk S, Alnasif A, Yu C, Thatcher J, Rudman J, Peronski L, et al. Combustion characteristics of a novel ammonia combustor equipped with stratified injection for low emissions. J Ammon Energy 2023;1:21–32.
[10] Bailey JC, Intile J, Fric TF, Tolpadi AK, Nirmalan NV, Bunker RS. Experimental and numerical study of heat transfer in a gas turbine combustor liner. J Eng Gas Turbine Power 2003;125:994–1002.
[11] Murai R, Omori R, Kano R, Tada Y, Higashino H, Nakatsuka N, et al. The radiative characteristics of $NH_3/N_2/O_2$ non-premixed flame on a 10 kW test furnace. Energy Procedia 2017;120:325–32.
[12] Murai R, Nakatsuka N, Higashino H, Akamatsu F. Review of fundamental study on ammonia direct combustion in industrial furnaces. In: Aika K-I, Kobayashi H, editors. CO_2 free ammonia as an energy carrier: Japan's insights. Singapore: Springer Nature Singapore; 2023. p. 627–40.
[13] Zheng J, Zhang X, Chung SH, Hu L. Experimental study on flame height and radiation characteristics in jet flames with ammonia/hydrocarbon mixture fuels. Combust Flame 2024;265:113517.

[14] Fang Y, Li G, Gao Y, Gong L, Liu Y, He P, et al. Effect of ammonia addition to hydrocarbon fuels on thermal radiation of turbulent diffusion jet flame. Int J Hydrog Energy 2024;78:1078–88.
[15] Nakamura H, Shindo M. Effects of radiation heat loss on laminar premixed ammonia/air flames. Proc Combust Inst 2019;37:1741–8.
[16] Fang R, Papas P, Sung C-J, Stevens JF, Smith LL. Effects of radiative heat loss on extinction limits of counterflow premixed ammonia-air flames. Proc Combust Inst 2024;40:105569.
[17] Zheng S, Liu H, Sui R, Zhou B, Lu Q. Effects of radiation reabsorption on laminar NH_3/H_2/air flames. Combust Flame 2022;235:111699.
[18] Zheng S, He Y, Hu B, Zhu J, Zhou B, Lu Q. Effects of radiation reabsorption on the flame speed and NO emission of NH_3/H_2/air flames at various hydrogen ratios. Fuel 2022;327:125176.
[19] Giacomo C, Guido M. The influence of radiation modeling on flame characteristics and emissions prediction in microcombustors with Ammonia/Hydrogen blends. Fuel (Lond) 2024:377.
[20] Sato D, Davies J, Lee S, Mashruk S, Valera-Medina A, Kurose R. Radiative characteristics of premixed coke oven gas-ammonia swirling flames. Fuel (Lond) 2025;401:135741.
[21] Davies J, Sato D, Mashruk S, Valera-Medina A. Experimental analysis of swirl number and nozzle design for scale-up of partially cracked ammonia flames. Appl Energy Combust Sci 2025;22:100338.
[22] Cafiero M, Dias V, Iavarone S, Coussement A, Jeanmart H, Parente A. Investigation of temperature correction methods for fine wire thermocouple losses in low-pressure flat premixed laminar flames. Combust Flame 2022;244:112248.
[23] Kramers H. Heat transfer from spheres to flowing media. Physica 1946;12:61–80.
[24] Coppalle A, Vervisch P. The total emissivities of high-temperature flames. Combust Flame 1983;49:101–8.
[25] Hottel HC, Egbert RB. The radiation of furnace gases. J Fluids Eng 1941;63:297–307.
[26] Kreith F, Bohn MS. Principles of heat transfer. Boston, MA: PWS Kent; 1997.
[27] Sellars J.R., Tribus M., Klein J.S. Heat transfer to laminar flow in a round tube or flat conduit 1954.
[28] Somarathne K, Hatakeyama S, Hayakawa A, Kobayashi H. Numerical study of a low emission gas turbine like combustor for turbulent ammonia/air premixed swirl flames with a secondary air injection at high pressure. Int J Hydrog Energy 2017;42:27388–99.
[29] Okafor EC, Naito Y, Colson S, Ichikawa A, Kudo T, Hayakawa A, et al. Measurement and modelling of the laminar burning velocity of methane-ammonia-air flames at high pressures using a reduced reaction mechanism. Combust Flame 2019;204:162–75.